Reduction of random noise from multiband image data using phase relationships among their Fourier coefficients

by J. V. Dave Jenö Gazdag

The problem of reducing the random noise from multiband image data is examined, taking a nine-band image data set of a terrestrial scene and adding a significant amount of noise to the original pixel value of each band. For each of these data sets, data of three nearby bands generally exhibit a high correlation among them. Selected data for several sets of three nearby bands are transformed from the spatial domain to the frequency domain to study phase relationships (i.e., coherency) among their Fourier coefficients of various frequencies. It is

**°Copyright** 1984 by International Business Machines Corporation. Copying in printed form for private use is permitted without payment of royalty provided that (1) each reproduction is done without alteration and (2) the *Journal* reference and IBM copyright notice are included on the first page. The title and abstract, but no other portions, of this paper may be copied or distributed royalty free without further permission by computer-based and other information-service systems. Permission to *republish* any other portion of this paper must be obtained from the Editor.

shown that, in general, the addition of random noise results in the rapid change, with frequency, of a quantity called the coherency measure. (This is a quantitative measure of the phase agreement among the phases of various Fourier coefficients at a given frequency.) The coherency measure vs. frequency curve for a given data line is then used to attenuate various Fourier coefficients of the corresponding nearby bands of that line. It is then shown that the inverse transformation of such modified Fourier coefficients results in a statistically significant reduction of noise from the data of single lines, or from those data of some finite areas of the image. Results of a supervised boxcar multispectral classification with the original as well as various modified data sets of the selected image are also presented to provide additional guidance in the use of such a sophisticated analytic procedure in image processing.

399

#### Introduction

Multiband digital image data of the terrestrial surfaces are routinely acquired in geological and geophysical explorations (e.g., [1]). Such measurements are generally taken with the help of multispectral scanners aboard aircraft or advanced spacecraft such as Landsat and Skylab. Such configurations generally provide data from 2 to 10 spectral regions (bands) in the visible near-infrared part of the electromagnetic spectrum, and that with a ground-level resolution of 8 to 80 m. Measurements for several spectral intervals in the 0.4-1.1-µm region are generally taken with the hope of determining and using unique spectral signatures of various types of surfaces. However, in practice, a great degree of redundancy develops due either to the nonexistence of such unique signatures, the coarseness of the spectral intervals, or the contamination of signals from stray light within the optical system. Because of any or all of these reasons, data of several nearby bands are generally found to be highly correlated.

This type of image data contains some noise due to various factors such as platform vibration, scene variability, atmospheric inhomogeneity, and digitization. Techniques for the reduction of noise from the image data are usually restricted to spatial smoothing confined to a single band. Smoothing along the wavelength direction is generally shunned because of the probability of obliterating some important image features.

One of the smoothing operations commonly used in signal processing and looked upon with some interest in image processing is the Fourier transformation of the data in a line or an area (i.e., one- or two-dimensional transformation) of the image in a given band [2, 3]. This transformation results in vectors with complex elements which represent the real image data in a spatial frequency domain. For the onedimensional transformation, the *n*th element of this complex vector for an image line gives the coefficient of the nth spatial frequency for that line. Since these coefficients are complex quantities, they contain magnitude as well as phase information. If the signal and noise are confined to different frequency ranges with some overlap, the Weiner filter [4] provides a weighting function determined by a least squares criterion of the accuracy of results. The complex coefficients can then be multiplied with the weighting function and the result can be inverse Fourier transformed to retrieve the filtered image data. However, it is very difficult to identify the frequency ranges dominated by signal and noise in the image data. Furthermore, especially for a large image, the determination of filter characteristics for individual scan lines becomes very time-consuming and costly.

The case of multiband data along an image line is, to some extent, analogous to that of multichannel space-time records (i.e., seismic traces) used in reflection seismology. In the latter field, additional assistance in the geophysical interpretation of seismic data is provided by computing a

coherency measure as a function of time, from the magnitude of the signals in different channels. Recently, Gazdag and Sguazzero [5] quantitatively defined a coherency measure to express the phase relationship among the Fourier coefficients of a given frequency. This coherency measure defined for the space-frequency domain can be used with significant advantage in the automatic extraction of the velocity information from the seismic traces.

In this report, we examine the problem of the reduction of random noise from the multispectral image-line data by Fourier-transforming them from the wavelength-space domain to the wavelength-frequency domain. A nine-band image (with 512 scan lines and 256 pixels per scan line) of a section of the Anadarko Basin of north central Oklahoma acquired in April 1979 with the Bendix Aerospace Modular Multispectral Scanner [6] is used for this purpose. The rectangular geometry of the image enables a split-screen comparison of the false-color images prepared with different procedures on the standard color monitors, while the 256-pixel length of a scan line permits the use of the efficient Fast Fourier Transform (FFT) method for the forward and inverse Fourier transformations [7, 8].

Variations of the coherency measure as a function of frequency are then studied for three different sets each of three nearby (or adjacent) spectral bands, and for several image lines with and without random noise added to the data. The sums of the elements of the coefficient vectors of the nearby bands are then multiplied by the corresponding elements of the coherency measure vector, and the resultant complex vector is inverse transformed to retrieve the image data for the middle of the three nearby bands. Results are then presented to show the role of the FFT operations and coherency measure in the reduction of random noise from the image line or image area data. Results of a supervised boxcar [9] multispectral classification performed with the original data, with the original data with random noise, and with both sets of data modified by two different procedures (viz. straightforward arithmetic mean of pixel radiances in nearby bands, and use of the FFT and coherency measure) are presented to provide additional justification and guidance for the use of such analytic procedures in image processing.

# **Fourier transformations**

Any real periodic function Y(x) can be expressed as a Fourier series of the form

$$Y(x) = a_0/2 + \sum_{n=1}^{\infty} \left[ a_n \cos (2\pi n \nu x) + b_n \sin (2\pi n \nu x) \right], \tag{1}$$

where  $\nu$  is the fundamental frequency. The same expression can be rewritten in exponential form by applying the identities representing these trigonometric functions in terms of complex exponentials.

400

Accordingly,

$$Y(x) = \sum_{n=0}^{\infty} \alpha_n \exp(\sqrt{-1} 2\pi n \nu x), \tag{2}$$

with

$$\alpha_n = 0.5(a_n - \sqrt{-1}b_n). \tag{3}$$

The phase angle  $\theta$  of the complex Fourier coefficient  $\alpha_n$  is given by

$$\tan \theta = b_n/a_n \,, \tag{4}$$

and with the appropriate quadrant for the vector determined from the signs of  $a_n$  and  $b_n$ .

The FFT (Fast Fourier Transform) is a very efficient procedure for transforming discrete data such as pixel values along an image line, especially when the number of data points can be represented by a power of 2 [8]. It is sufficient to state here that a periodic function is developed using  $2^m$  measurements. It is then analyzed to derive  $2^m$  complex coefficients  $\alpha_n$ . For the real data of concern to us in the present context,  $a_{-n} = a_n$ , and  $b_{-n} = -b_n$ . We therefore restrict our discussion to the coefficients with zero and positive subscripts only. For convenience, it is customary to refer to the  $\alpha_0$  coefficient as the amplitude of the first frequency. Thus, for an image with 256 pixels per line, we are interested in phase relationships among the Fourier coefficients of various bands for the first 129 frequencies only.

Following [5], we define the coherency measure  $\Gamma_{n,K}$  among the *n*th frequency Fourier coefficients of three bands, K-1 to K+1, by the equation

$$\Gamma_{n,K} = \frac{\left| \sum_{k=K-1}^{K+1} \alpha_{n,k} \right|^2}{\left[ \sum_{k=K-1}^{K+1} |\alpha_{n,k}| \right]^2},$$
(5)

where  $\alpha_{n,k}$  is the *n*th-frequency Fourier coefficient for the data of the *k*th band. This coherency measure assumes a value of unity if all  $\alpha_{n,k}$  for a given *n* are in phase [see Eq. (4)], and a value very close to zero if their phases are randomly oriented.

A basis for the use of this coherency measure as a filter is given in the next section. Accordingly, we accept the quantity  $\Gamma_{n,K}$  defined by Eq. (5) as the scalar attenuation factor for the coefficients of K-1 to K+1 bands at the *n*th frequency. Then the modified Fourier coefficient  $\beta_{n,K}$  for the Kth band is given by

$$\beta_{n,K} = \left[ \Gamma_{n,K} / 3 \right] \sum_{k=K-1}^{K+1} \alpha_{n,k} . \tag{6}$$

Thus, we have an automatic determination of the filter vector  $\Gamma_{n,K}$  for a weighting of all coefficients for K-1 to K+1 bands. The modified (or attenuated) coefficients ( $\beta_{n,K}$  for

various n) can then be inverse transformed to obtain the Kth-band modified data for the image line under scrutiny.

In the image science discipline, pixel radiances are usually represented by an eight-bit (byte) word which ranges from 0 to 255. The inverse transform of the complex  $\beta_{n,K}$  vector results in another complex vector whose real parts represent the modified pixel radiances. In order to conform to one-byte representation, real parts of this other complex vector are forced to 0 if they are negative and to 255 if they are greater than 255.

If the quantity  $\Gamma_{n,K}$  is equal to unity for all values of n for a given K, the combined process of the forward Fourier transform, the filtering of the Fourier coefficients, and the inverse Fourier transform of the resultant vector is equivalent to taking the arithmetic mean of the radiances of a pixel, in the selected line, in K-1 to K+1 bands.

# Filtering of multichannel data using coherency measures

Let

$$r_{\nu}(x) = s(x) + n_{\nu}(x)$$
  $k = 1, 2, \dots, K$  (7)

denote K independent observations or measurements of the same event; the quantities s(x) and  $n_k(x)$  denote the signal and noise components of the observation, respectively. It can be thought of as a correlated subset of the multispectral data along a straight line defined over the image domain, where x is the distance along the line. Let  $\alpha_{n,k}$  be the Fourier transform of  $r_k(x)$  given by

$$\alpha_{n,k} = \sum r_k(x) \exp(\sqrt{-1} 2\pi n \nu x), \tag{8}$$

where the summation is carried out over all samples  $x = l\Delta x$ , and l assumes integer values between 0 and some upper limit 2L. The Fourier coefficients  $\alpha_{n,k}$  are computed for angular frequencies  $-\pi/\Delta x$  to  $+\pi/\Delta x$ .

Following Eq. (7), the Fourier coefficients can also be thought of as those due to signal and noise, i.e.,

$$\alpha_{nk} = S_n + N_{nk} \,. \tag{9}$$

 $S_n$  is independent of the subscript k (i.e., spectral band number), while  $N_{n,k}$  varies from band to band. Evidently, both of these quantities are also complex. When  $\alpha_{n,k}$  is summed over all values of k, the summation over  $S_n$  is  $KS_n$  but the sum of the uncorrelated noise vectors gives a composite vector that is less than the sum of their absolute values; i.e.,

$$\left| \sum_{k=1}^{K} N_{n,k} \right| < \sum_{k=1}^{K} |N_{n,k}|. \tag{10}$$

These considerations suggest a quantitative measure for discriminating among the Fourier coefficients that represent signal as well as noise. Gazdag and Sguazzero [5] have shown that the ratio between the absolute value of the sum of vectors, and the sum of the absolute values thereof, is an

401

**Table 1** Nominal bandwidths of various spectral bands available on the airborne Modular Multispectral Scanner (Lowe, 1980).

Band number	Nominal spectral width (µm)	Descriptive color
1	0.38-0.44	violet
2	0.44-0.49	blue
3	0.49-0.54	green
4	0.54-0.58	greenish yellow
5	0.58-0.62	orange
6	0.62-0.66	red
7	0.66-0.70	red
8	0.70-0.74	red-infrared
9	0.76-0.86	infrared
10	0.97-1.05	infrared
11	8.00-12.00	thermal infrared

effective measure of the collective phase agreement among the  $\alpha_{n,k}$  for a given n. Accordingly, the quantity  $\Gamma_n$  [the second subscript K is omitted here for brevity; see Eq. (5)], which is defined by

$$\Gamma_{n} = \frac{\left|\sum \alpha_{n,k}\right|^{2}}{\left[\sum \left|\alpha_{n,k}\right|\right]^{2}},\tag{11}$$

can be regarded as the measure of coherency. This is because  $\Gamma_n$  attains its maximum value of unity if all the  $\alpha_{n,k}$  for a given n have the same direction; i.e., they have the same phase angle, implying that they are coherent. As the phase agreement among the  $\alpha_{n,k}$  for a given n decreases,  $\Gamma_n$  also decreases, and it eventually becomes close to zero when these coefficients are randomly oriented; i.e., they are out of phase.

The coherency measure  $\Gamma_n$  as defined by Eq. (11) can be used to improve the signal-to-noise ratio of any band provided that this filtering operation consists of multiplying the Fourier transform of the kth band by  $\Gamma_n$ . Let the signal-to-noise ratio be defined as the ratio of their respective energies, i.e.,

$$SNR_k = \sum S_n^2 / \sum N_{nk}^2, \tag{12}$$

when the summation is carried out over all values of n. Let us now examine the effect of multiplying  $\alpha_{n,k}$  with  $\Gamma_n$  given by Eq. (11). Since  $\Gamma_n$  is applied to both  $S_n$  and  $N_{n,k}$ , the signal-to-noise ratio of the processed signal is given by

$$SNR_{k}^{*} = \sum \left[ S_{n} \Gamma_{n} \right]^{2} / \sum \left[ N_{n,k} \Gamma_{n} \right]^{2}. \tag{13}$$

Since  $\Gamma_n$  attains higher values for those frequencies that are least contaminated by noise and vice versa, its correlation with the signal component is expected to be greater than that with the noise component. It can therefore

be shown that the normalized signal given by

$$\sum \left[ S_{n} \Gamma_{n} \right]^{2} / \sum S_{n}^{2} \sum \Gamma_{n}^{2} \tag{14}$$

is greater than the normalized noise given by

$$\sum \left[N_{n,k}\Gamma_n\right]^2 / \sum N_{n,k}^2 \sum \Gamma_n^2. \tag{15}$$

From this inequality relationship, it can be easily shown that  $SNR_{\nu}^{*}$  is greater than  $SNR_{\nu}$ .

The improved signal-to-noise ratio obtained by multiplying the Fourier coefficients of a signal with the corresponding  $\Gamma_n$  need not be restricted to the individual bands. This approach can also be taken for the composite signal resulting from the summation of all bands under consideration. For the type of data used in our investigation, the latter approach was found to be more satisfactory than the first one.

### Multispectral classification

The multispectral classification procedure used in our analysis is a modified form of the standard boxcar or parallelepiped classification scheme [9]. Classes are numbered in powers of 2, i.e., 1, 2, 4, 8, and so on. With this modified form, the results are independent of the order in which the classes are specified.

The count-range  $C_{j,k}$  for the kth band and the jth class is determined from the histogram of the radiance of the pixels in the training site for that class. For our work, this countrange is defined as the range containing 90 percent of the total pixels in the training site. If the values of a pixel in bands  $b_1, b_2, \dots, b_k$  are located within the corresponding count-ranges  $C_{j,1}, C_{j,2}, \dots, C_{j,k}$ , the pixel is said to belong to the jth class.

Before setting up the classification procedure, all of the elements of a matrix of the size of the image are set to zero. Then, if a pixel is judged to belong to a given class, the corresponding class number is added to the contents of the corresponding element of the matrix. If a pixel is judged to belong to more than one class, the corresponding matrix element carries a value of the sum of the number of all classes to which that pixel is found to belong. For the eight-class classification, we have a total of 256 classes, viz., the first for the unidentified pixels, the next eight for the eight original classes specified by the investigator, and the remaining 247 possible mixed classes containing pixels belonging to any two or more of the eight classes.

### **Basic data sets**

The first basic data set used in our investigation was extracted from data acquired in April 1979 (with the help of the Modular Multispectral Scanner [6]) over the Anadarko Basin of north central Oklahoma. Nominal spectral bandwidths of the eleven channels recorded by this instrument are shown in **Table 1**. It can be seen that the first

nine bands are located in the visible near-infrared  $(0.38-0.86 \mu m)$  part of the electromagnetic spectrum. From a full flight-line data set consisting of 3800 scan lines with 803 pixels per scan line, a subset consisting of 512 scan lines with 256 pixels per scan line was selected as the first basic data set for our investigation.

A black and white photograph of a false-color image of the selected area, prepared after linear contrast-stretch operations on the data of bands 2, 5, and 8, is shown in the left half of **Figure 1**. The selected region contains eight to ten different features such as water, small hills, and fields in different stages of growth. The pixel size for this area is about 8-10 m.

For this image, data for bands 10 and 11 were found to be very highly correlated (correlation coefficient of 0.99) and had practically the same values for mean brightness and standard deviation. Therefore, data of these two bands were omitted in further analysis. Another reason for omission of these two bands is the desire to obtain three-band false-color images after each operation on the data. Consistency considerations then require working with nine or 15 bands [see Eq. (5)]. For the first nine bands, the correlation coefficient of the first band data with any of the remaining bands was found to decrease with an increase in band order from 0.98 to -0.3. The correlation coefficient of the image data for the second band with those of any two nearby bands (i.e., first and third bands) was found to be about 0.95. The same high correlation was also observed for the data of the fifth band with those of its nearby bands. On the other hand, the values of band 8 were found to be highly correlated (≈0.9) with those of band 9, but only weakly correlated  $(\cong 0.5)$  with those of band 7. Thus, the selection of values of 2, 5, and 8 for the subscript K appearing in Eq. (5) provides us with several significantly different cases of phase relationships among the multiband Fourier coefficients of various frequencies.

Various types of analysis of this first basic data set suggested the data to be, relatively speaking, free of random noise. Therefore, a second basic data set was generated by adding random noise (range:  $\pm 20$  units) to each of the 131 072 (=  $256 \times 512$ ) pixel values of each of the nine bands. Original pixel radiances are given in arbitrary units and, because of the one-byte representation mentioned earlier, they can carry any value in the range 0–255. Therefore, the addition of  $\pm 20$  units of random noise, though somewhat arbitrary, is quite significant from the quantitative point of view. The histogram of the random noise values added to any image band is flat for all practical purposes.

A black and white photograph of the false-color image, prepared after linear contrast-stretch operations on the data of bands 2, 5, and 8 of this second set (i.e., with random noise), is shown on the right-hand side of Fig. 1. A trained eye can detect some subtle differences between the original

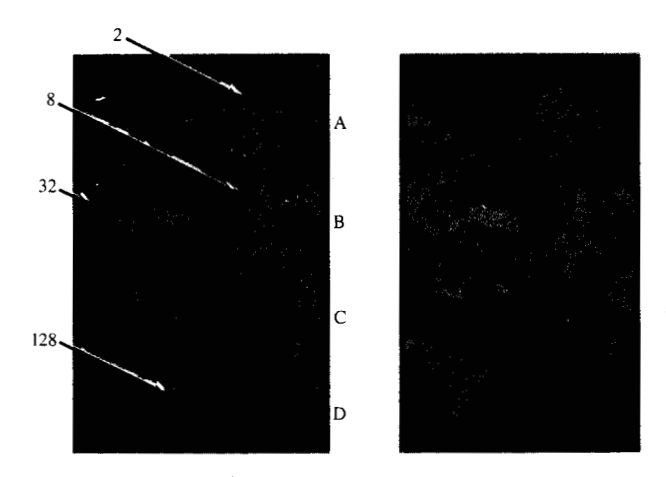


### Figure 1

A black and white photograph of the three-band false-color image of a small section of the Anadarko Basin of north central Oklahoma. Left: original data; right: with random noise (range: ±20 units) added to each pixel value of each band.

and noisy black and white images shown in this figure; there is also some degradation in quality.

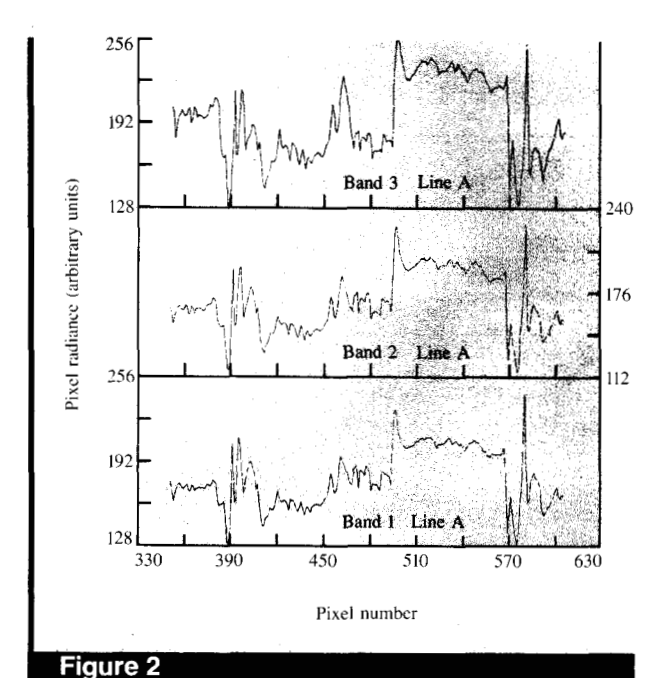
Line and area regions of the selected image used in the quantitative analysis are shown in the left half of Fig. 1. There are four lines designated A, B, C, and D, and eight polygon areas used as training sites for the multispectral classification. These areas are numbered 1, 2, 4, 8, 16, 32, 64, and 128. Some of these identification marks are omitted for clarity.

Variations of the pixel radiance (in arbitrary units) as a function of its position on the lines A and B in Fig. 1 are shown in Figures 2 and 3, respectively, for a few selected bands. The x-axis parameter refers to the pixel number which referred to the data in the original data set from which the image was extracted. The left and right ends of the curves in these diagrams correspond to the left and right edges of the left half of Fig. 1, respectively. From the data presented in Fig. 2 for bands 1–3, we see that the measurements of these three bands are highly correlated. However, from the data presented in Fig. 3 for bands 7–9, we find a fairly good correlation among measurements of bands 8 and 9, but a somewhat weak correlation for those of bands 7 and 8.

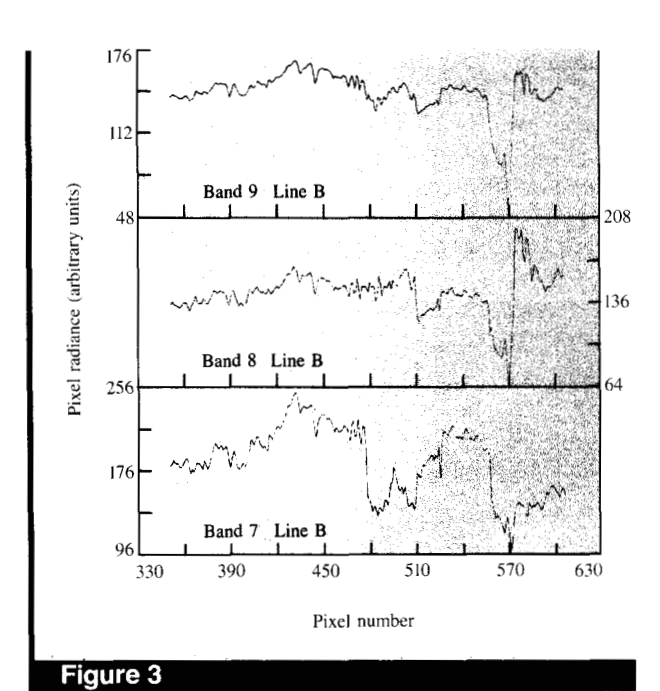
#### Phase relationships

As mentioned earlier in the section on Fourier transformations, FFT operations on data of a given band of a given line with 256 pixels provide independent complex Fourier coefficients for 129 frequencies.

Phase relationships among the Fourier coefficients of eight selected frequencies of data of bands 1–3 of line A (see Fig.



Variations of the pixel radiance in bands 1, 2, and 3, as a function of its position on line A in Fig. 1.



Variations of the pixel radiance in bands 7, 8, and 9, as a function of its position on line B in Fig. 1.

2), and of data of bands 7-9 of line B (see Fig. 3), are shown in Figures 4 and 5, respectively. In each case, the results for

the first (i.e., original) and second (i.e., with the random noise added) data sets are shown in the left half and right half of the figure, respectively. Thus, there are 16 squares in each figure. Appropriate frequency numbers are shown in the top left corner of the squares. Values of  $a_{n,k}$  and  $b_{n,k}$ , required in computations of a given  $\Gamma_{n,K}$ , are divided by the maximum of the absolute values of that particular set. This maximum value, later referred to as the normalization factor, is shown in the bottom left corner of the square. The computed value of  $\Gamma_{n,K}$  is given in the bottom right corner. Coefficient vectors of the K-1, K, and K+1 bands are shown by the solid, broken, and dotted lines, respectively.

From the results presented in Fig. 4 for the data of bands 1 to 3, it can be seen that the addition of random noise results in a separation of the vectors and a decrease in the coherency measure  $\Gamma_{n,2}$ . The only exception to this statement is the 67th frequency, for which the normalization factor is very small. On the other hand, several values of  $\Gamma_{n,8}$  (see Figure 5) increase by a significant amount with the addition of the random noise to the original data. Some of these trends may be due to the weak correlation among the values of bands 7 and 8 mentioned earlier, or due to the presence of some significant amount of noise in the first set.

### **Coherency measure variations**

Variations of  $\Gamma_{n,2}$  for line A, of  $\Gamma_{n,8}$  for line B, and of  $\Gamma_{n,2}$  and  $\Gamma_{n,8}$  for line D are shown, as a function of frequency n, in Figures 6, 7, 8, and 9, respectively. Each of these figures consists of two sections with the results for the data of the first and second basic set shown in the bottom and top sections, respectively.

From the results presented in Fig. 6 for  $\Gamma_{n,2}$  vs. n for line A, the effect of random noise on the values of  $\Gamma_{n,2}$  at higher frequencies is very evident. Such an effect is also present, to some extent, in variations of  $\Gamma_{n,8}$  vs. n for line B shown in Fig. 7. As one would anticipate, such variations are highly data-dependent. Variations of  $\Gamma_{n,2}$  vs. n for line D (see Fig. 8) show a strong decreasing trend at higher frequencies in the lower section, but a very weak decreasing trend, if any, in the upper section of the diagram. On the other hand, variations of  $\Gamma_{n,8}$  vs. n for line D (see Fig. 9) show several very significant cases of decrease in  $\Gamma_{n,8}$  with the addition of random noise.

# Procedures 1 and 2

Computations of the Fourier coefficients and of the modified image data from them, for the multiband cases, require a fairly significant amount of computational resources. It is therefore advisable to compare the results obtained after such sophisticated operations with those obtained with the one requiring minimal operations. With this in mind, we have defined procedures 1 and 2 as follows.

In procedure 1, an arithmetic mean of the radiances of an image pixel in bands K - 1, K, and K + 1 is taken;

# Figure 4

respectively. frequency, the normalization factor, and the coherency measure, left corner, the three values in a given square represent the band. Proceeding in the counterclockwise direction from the top random noise (range: ±20 units) added to each pixel value of each half: relationships for the original data; right half: relationships with frequencies of the data of bands 1, 2, and 3 of line A in Fig. 1. Left Phase relationships among the Fourier coefficients of eight selected

0.9782

96/60

5230

99

/Z 02

296.811

133.654

116.487

73.377

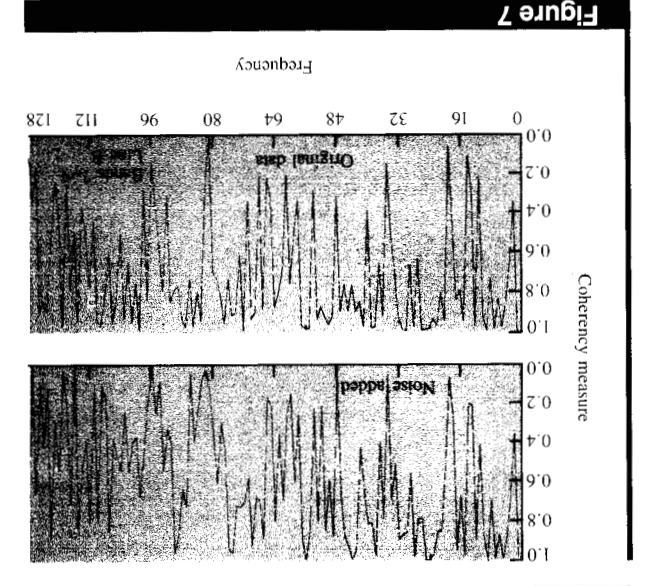
9928'0

ECLEO

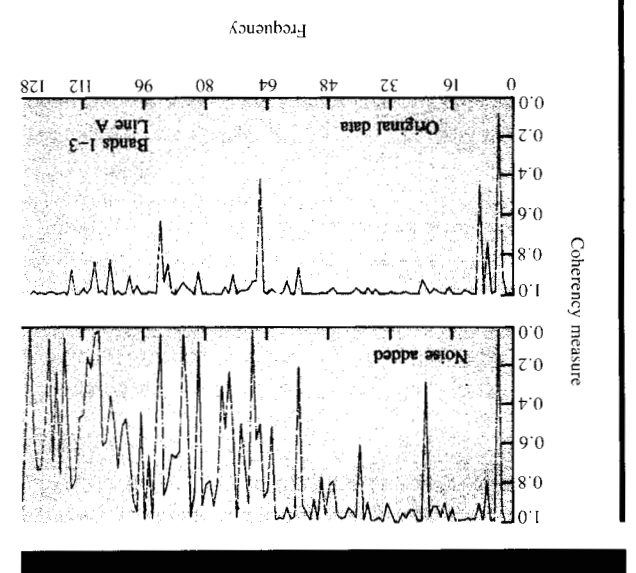
8910.0

# Figure 5

respectively. frequency, the normalization factor, and the coherency measure, left corner, the three values in a given square represent the band. Proceeding in the counterclockwise direction from the top random noise (range: ±20 units) added to each pixel value of each half: relationships for the original data; right half: relationships with frequencies of the data of bands 7, 8, and 9 of line B in Fig. 1. Left Phase relationships among the Fourier coefficients of eight selected

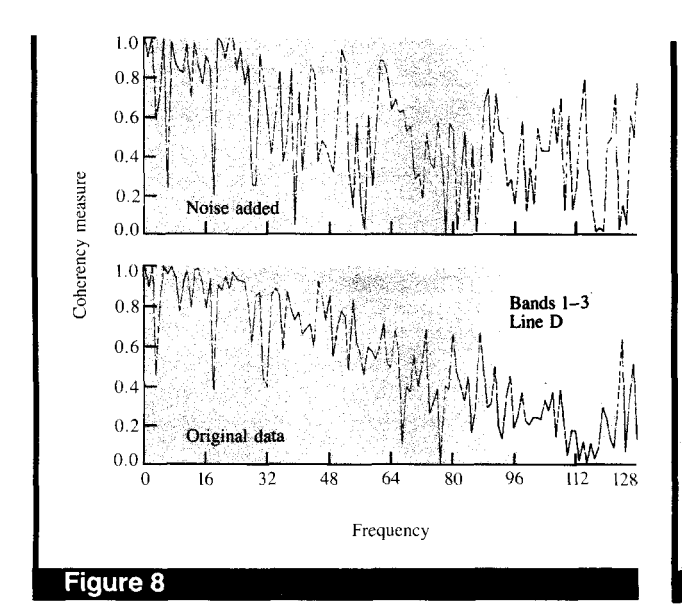


each pixel value of each band. original data; top: after random noise (range:  $\pm 20$  units) is added to among the data of bands 7, 8, and 9 of line B in Fig. I. Bottom: Variations of the coherency measure, as a function of the frequency,



each pixel value of each band. among the data of bands I, 2, and 3 of line A in Fig. I. Bottom: original data; top: after random noise (range:  $\pm 20$  units) is added to Variations of the coherency measure, as a function of the frequency,

Figure 6



Variations of the coherency measure, as a function of the frequency, among the data of bands 1, 2, and 3 of line D in Fig. 1. Bottom: original data; top: after random noise (range:  $\pm 20$  units) is added to each pixel value of each band.

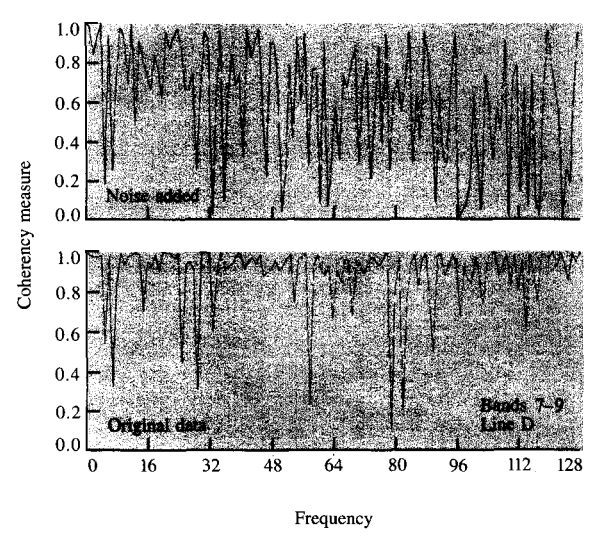
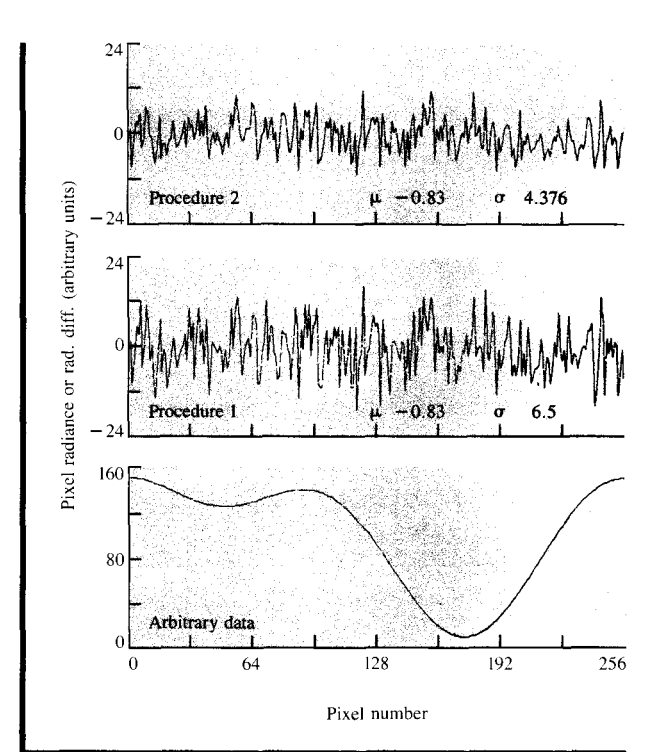


# Figure 9

Variations of the coherency measure, as a function of the frequency, among the data of bands 7, 8, and 9 of line D in Fig. 1. Bottom: original data; top: after random noise (range:  $\pm 20$  units) is added to each pixel value of each band.



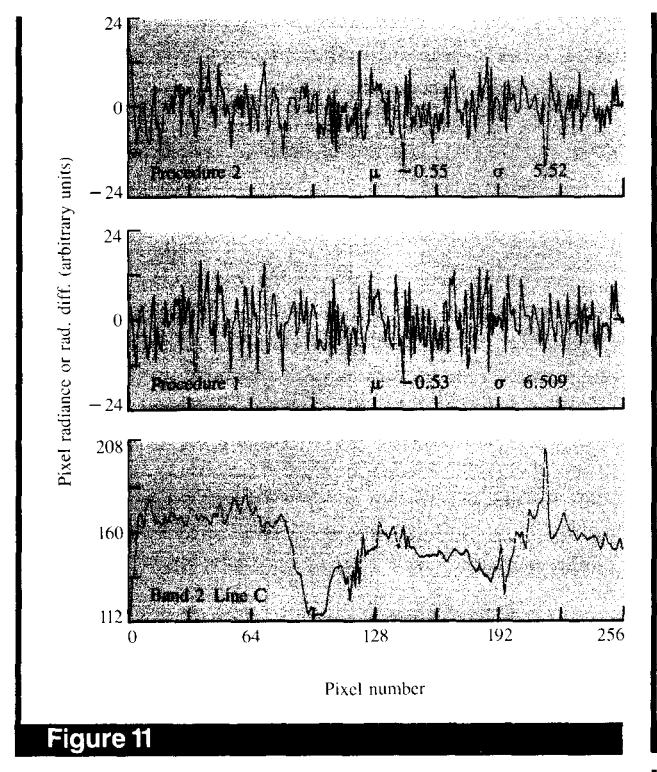
Variations, as a function of the pixel position, of the pixel radiance (arbitrary data without any noise), and of the random noise remaining after procedures 1 and 2 (middle and top sections, respectively) are applied to three data sets generated after adding random noise to the original data.

evidently, K equals 2, 5, and 8. In procedure 2, real data of an image line in bands K-1, K, and K+1 are transformed from the spatial domain to the frequency domain, and complex Fourier coefficients are computed for each band. A filter is then computed automatically by making use of Eq. (5). The modified Fourier coefficients [see Eq. (6)] are then inverse-transformed to obtain the modified image data for the Kth band. This procedure is then repeated for each line of the image.

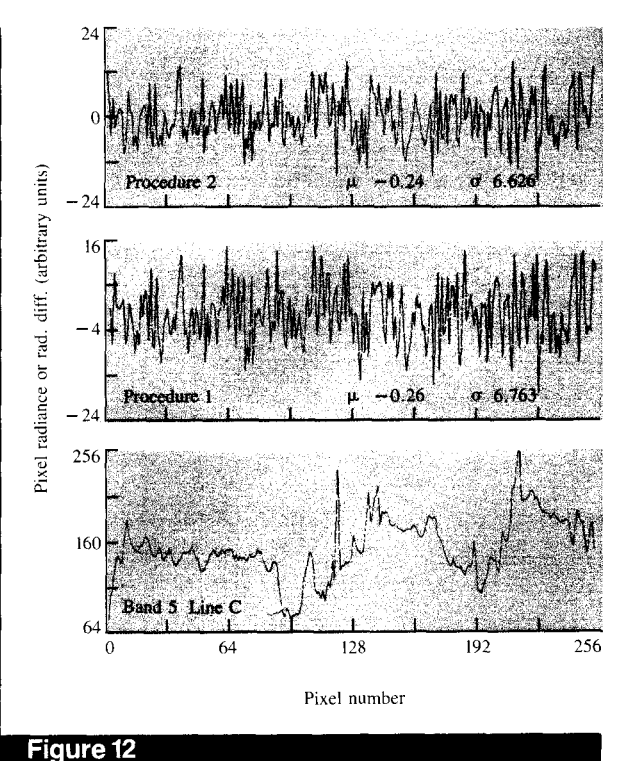
### Noise reduction for the single-line cases

The lowest section of Figure 10 shows the variations of pixel radiance along a line with some arbitrary data generated by taking into account only the first three Fourier components. A random noise of  $\pm 20$  units was then added to this arbitrary data line, and three more lines with noisy arbitrary data were generated. Procedures 1 and 2 were then applied to these three-line data treated as three-band data. Differences between the pixel values obtained with procedures 1 (and 2) and the original line data are plotted in the middle (and the upper) sections of Fig. 10. In other words, these two curves represent the random noise remaining after application of the corresponding smoothing procedure. The statistical parameters of the mean brightness  $(\mu)$  and the standard deviation  $(\sigma)$  for the added noise are about -0.77 and 10.97, respectively. The value of  $\sigma$ decreases to 6.5 and 4.4 after application of smoothing procedures 1 and 2, respectively. Thus, it can be seen that the second procedure does provide better smoothing than

Figure 10



Variations, as a function of the pixel position, of the pixel radiance (original data of band 2, line C in Fig. 1), and of the random noise remaining after procedures 1 and 2 (middle and top sections, respectively) are applied to three data sets generated after adding random noise to the original data.



Variations, as a function of the pixel position, of the pixel radiance (original data of band 5, line C in Fig. 1), and of the random noise remaining after procedures 1 and 2 (middle and top sections, respectively) are applied to three data sets generated after adding random noise to the original data.

the first, especially when the signal is confined to a few lower frequencies only.

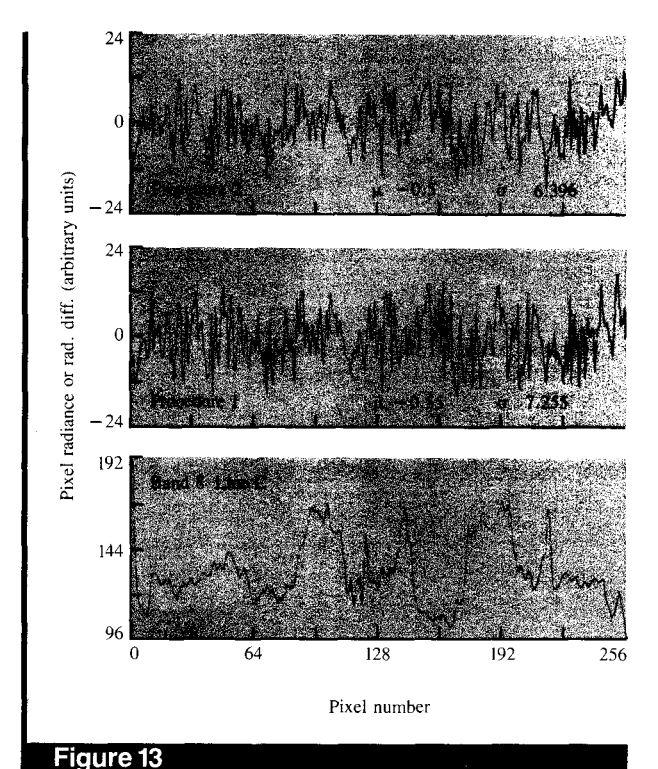
It can be shown that the decrease in  $\sigma$  for the random noise after the use of procedure 1 is in agreement with what can be expected from the consideration of the wave energy which is proportional to the square of the amplitude. If three identical waves (or signals) are added and the resultant wave is integrated over a sufficiently large interval of its independent variable, its energy increases by a factor of 9 over that of a single wave. On the other hand, if these three waves carry some random noise, the integrals over the product terms can be expected to vanish over a sufficiently large interval of integration. Accordingly, the energy of the resultant wave in this latter case is about three times greater than that of any single wave. Thus, the gain is about 3 in energy, or the square root of 3 in the case of amplitude of the wave. Assuming that the standard deviation values provided in the preceding paragraph are related to the noise amplitudes, we have an improvement by a factor of 10.97/6.5 = 1.69, which is comparable to the square root of 3. A still better improvement can be obtained by taking more than three sets.

Results similar to those presented in Fig. 10 but for the actual image data along line C in Fig. 1 are shown in **Figures 11, 12,** and **13** for bands 2, 5, and 8, respectively. The respective standard deviations in the original random noise are about 11.6, 11.4, and 11.9 for these three cases. From the values of  $\sigma$  given inside these figures, it can be seen that in general the application of procedure 2 results in a better reduction in random noise than that of procedure 1. However, the improvement is not as large as in the case of data with signals confined to the low frequency only (i.e., results of Fig. 10).

# Noise reduction for the training sites

For the results presented in the preceding section, three lines of data with random noise were generated from the original line data for the selected band. On the other hand, results presented in this and the following sections were obtained after the use of procedure 1 or 2 as defined earlier.

For multispectral classification analysis, we have selected eight training sites whose class numbers are given in powers of 2, i.e., 1, 2, 4, 8, and so on. The total number of pixels in each of these training areas is given in column 3 of **Table 2**.



Variations, as a function of the pixel position, of the pixel radiance (original data of band 8, line C in Fig. 1), and of the random noise remaining after procedures 1 and 2 (middle and top sections, respectively) are applied to three data sets generated after adding random noise to the original data.

This table consists of two sections with the  $\sigma$  values for bands 2 and 8 given in columns 4 through 7 of its upper and lower sections, respectively. Column 4 contains the standard deviation for the original (i.e., basic data set without any noise added to it) radiances of the pixels inside the training areas. Similar results, but with  $\pm 20$  units of random noise added to each pixel value of each band (i.e., basic data set 2), are given in column 5 of this table. It can be seen that the addition of the random noise results in a significant increase in the standard deviation in all cases.

Values of the standard deviation obtained after application of procedures 1 and 2 are shown in columns 6 and 7, respectively. The use of either smoothing procedure results in a significant reduction of the noise level (as interpreted from a decrease in the standard deviation) in all cases. The second procedure provides lower values of  $\sigma$  than the first procedure for all eight training areas for band 2, but not for band 8.

# Multispectral classification results

One of the main purposes in the acquisition and analysis of multiband image data in geophysical and agricultural exploration is to identify areas (i.e., pixels) with the same optical characteristics as those of the selected training sites. Such identification assists in the location of other regions of economic importance. In the boxcar multispectral classification, these characteristics are specified by the countranges. Even though an improvement in the quality of the results obtained after the application of a particular procedure to the image data can be readily associated with a

**Table 2** Total number of pixels in the training sites of various classes, and the standard deviation ( $\sigma$ ) for their band 2 and band 8 data.

Band number	Class number	Number of pixels	σ for the original data	σ after adding random noise	σ after applying Proc. I	σ after applying Proc. 2
2	1	1008	5.74	8.24	6.93	6.45
2	2	1037	3.28	6.57	4.87	4.67
2 2 2 2	4	305	6.06	8.49	7.12	6.47
2	8	409	1.96	6.18	4.43	4.06
2	16	593	4.46	7.12	5.57	5.11
2	32	728	5.94	8.02	7.24	6.74
2	64	44	4.21	7.90	6.74	6.45
2	128	595	9.18	10.87	9.84	8.97
8	i	1008	3.41	6.64	4.92	5.03
8	2	1037	3.17	6.63	5.05	5.53
8	4	305	18.98	19.97	12.68	11.18
8	8	409	4.24	6.61	5.98	5.96
8	16	593	5.79	8.11	5.30	4.92
8	32	728	5.50	8.25	7.79	6.33
8	64	44	2.85	7.54	6.03	6.09
8	128	595	5.45	8.02	5.51	5.02

decrease in the standard deviation (or the count-range width), it is not possible to determine the quality of the classification products without access to the detailed ground-truth information about the scene at the time of observation. Differences in the number of pixels assigned to a particular class with two different mathematical operations on the data cannot be used in the judgment of their relative merits. If one operation results in the random geographic distribution of pixels assigned to a given class (the so-called salt-and-pepper effect), one can assign a lower figure of merit to that operation. However, the determination of the randomness of a given geographic distribution of pixel positions is likely to be subjective unless sophisticated mathematical procedures are used for this purpose.

When the different multispectral classification products obtained with two different mathematical operations on the data are compared, one can find any or all of the following three cases:

- 1. A pixel is assigned to the same class in both products.
- A pixel is assigned to a given class in one product, but to no class in the second product.
- A pixel is assigned to one class in one product, but to some other class in the second product.

The classification results obtained after different operations on the data were analyzed in such detail. However, it was not possible to arrive at any definite conclusion about the relative figures of merit of various operations. With this in mind, only a few selected results of the classification product comparison are reproduced in this section.

Tables 3 and 4 contain the number of pixels assigned to a given class when the original (i.e., noise-free, basic data set 1) and the noisy (i.e., with  $\pm 20$  units of random noise, basic data set 2) data are used in the multispectral classification, respectively. Each table consists of five columns with the class number given in the first column. For the noise-free case, we have eight original classes, plus a mixed class 40 due to the assignment of the same pixel to class 8 and class 32. An additional mixed class (No. 129) appears after random noise is added to the data (see Table 4).

The results presented in columns 2 and 3 of Tables 3 and 4 were obtained after making use of the data of all nine bands, and those of bands 2, 5, and 8 only, respectively. The use of all nine bands in multispectral classification leads to rather drastic constraints, which in turn results in a smaller number of pixels being assigned to a given class. Furthermore, no pixels are assigned to mixed class 40 for the

Furthermore, no pixels are assigned to mixed class 40 for the nine-band noise-free case, but 110 pixels are assigned to this mixed class for the three-band noise-free case. The addition of random noise to the data results in the assignment of 194 pixels to class 40 for the nine-band case, and the insurgence of mixed class 129 with 1181 pixels for the three-band case.

**Table 3** Results of the modified boxcar multispectral classification as obtained with the original data.

Class number	All nine bands	Bands 2, 5, and 8	Procedure 1	Procedure 2
1	3,851	6,023	7,702	7,864
2	3,585	4,294	4,643	4,381
4	1,448	1,780	1,825	1,770
8	1,614	2,276	1,638	2,097
16	1,644	2,216	2,406	2,829
32	4,220	5,490	7,078	6,707
64	152	188	314	317
128	14,331	20,187	18,167	18,124
40	0	110	920	183

**Table 4** Results of the modified boxcar multispectral classification as obtained with the noisy (i.e., with  $\pm 20$  units of random noise added to each original pixel value of each band) data.

Class number	All nine bands	Bands 2, 5, and 8	Procedure 1	Procedure 2
1	4,937	11,154	10,441	10,653
2	2,983	5,687	5,204	4,850
4	1,368	2,080	1,930	1,731
8	1,259	2,081	1,654	2,328
16	1,454	3,416	2,745	2,847
32	4,009	7,245	7,549	7,032
64	236	811	562	477
128	14,145	24,171	20,178	19,776
40	194	1,566	1,719	838
129	0	1,181	0	0

The results of the multispectral classification with image data smoothed after the application of procedures 1 and 2 are given in columns 4 and 5, respectively, of these two tables. It is interesting to note that the application of the second procedure results in the assignment of fewer pixels to the mixed classes, i.e., fewer doubtful pixels. To that extent, one can state that there are some advantages in the use of the sophisticated procedure 2 over that of the simple-minded procedure 1.

In **Table 5**, the results of an analysis are presented to show the number of pixels that can be assigned to the same class before and after the addition of random noise. Identical operations (viz. nine-band, three-band, or procedure 1 or 2) are performed in both cases. Again, it can be seen that, on the average, the use of the second procedure results in the reassignment of more pixels to the same class. However, whether the additional effort required in Fourier transformation is worth the gain or not remains debatable.

### Concluding remarks

In the preceding sections, the reduction of random noise from multiband image data with a good degree of correlation

**Table 5** Number of pixels that can be reassigned to the same class after ±20 units of random noise is added to each pixel value of each band, and identical operations are performed to obtain the multispectral classification results in both cases.

Class number	All nine bands	Bands 2, 5, and 8	Procedure 1	Procedure 2	•		
1	2,702	4,715	6,579	6,868			
2	2,317	3,549	4,033	3,723			
4	1,107	1,611	1,603	1,501			
8	884	1,140	1,036	1,580			
16	1,046	1,824	2,033	2,272			
32	2,871	3,983	5,604	5,424			
64	104	174	275	276			
128	10,804	16,784	16,049	16,162			
Totals	21,835	33,780	37,212	37,806			

among the nearby bands is examined in several alternate manners. A  $256 \times 512$  nine-band image data set acquired with the aircraft-mounted multispectral scanner was used for this purpose. For this numerical experiment, an additional data set was generated by adding a significant amount of random noise to each measured value in each spectral band. Two different smoothing procedures were used in our analysis: 1) arithmetic means of pixel values in bands K-1, K, and K+1 with K=2, 5, and 8; and 2) one-dimensional Fourier transformation of the image data in the K-1, K, and K+1 bands, automatic development of a filter based on the phase coherency of the Fourier coefficients in these three bands, and the use of the inverse Fourier transformation to obtain the data with a reduced noise level.

It has been shown that the application of the second smoothing procedure results in a significant reduction of the noise level in most cases. The results of a modified boxcar multispectral classification on the original as well as on the noisy data smoothed using these procedures are also presented to show the degree of improvement that can be achieved in various cases. Conclusions derived from these latter tests are, to some extent, inconclusive because of the unavailability of the ground-truth information at the time of observation. However, this is the first known attempt at smoothing the correlated multiband image data using the phase relationships among various bands. Its findings are encouraging enough to justify further investigations on the potential of this technique. This may include the collection of extensive ground-truth information at the time of imaging, or the generation of simulated data sets providing 100 percent ground truth.

As mentioned earlier, we have restricted ourselves to a one-dimensional transformation of the data from the spatial to the frequency domain, and back to the spatial domain after the appropriate weighting of the Fourier coefficients. It is expected that such transformations in two dimensions will

provide still better results. In the discussion of the results presented in Fig. 10, it was implied that the level of improvement would increase with an increase in the number of bands. Therefore, this technique may offer some advantages in the analysis of very poor-quality sequential images of the same scene, e.g., some medical images. The smoothing procedures developed for our investigation also offer alternate tools for the reduction of the dimensionality of the multidimensional data sets. It may therefore be of some interest to compare the results of such smoothing procedures with those obtained with the well-known principal component analysis [10].

### Acknowledgments

We would like to take this opportunity to express our sincere thanks to Harwood G. Kolsky and Alan H. Karp of the IBM Palo Alto Scientific Center, and to Michael A. Wiley of the Research and Development Department of ARCO Oil and Gas Company, Plano, Texas, for their valuable assistance at various stages of this undertaking. The image data used in our investigation were acquired by the ARCO Oil and Gas Company, Dallas, Texas, and were kindly made available to the authors under a joint study.

### References

- B. S. Siegal and A. R. Gillespie, Eds., Remote Sensing in Geology, John Wiley & Sons, Inc., New York, 1980.
- R. Bracewell, The Fourier Transform and Its Applications, McGraw-Hill Book Co., Inc., New York, 1965.
- W. K. Pratt, Digital Image Processing, John Wiley & Sons, Inc., New York, 1978.
- G. C. Newton, Jr., L. A. Gould, and J. F. Kaiser, Analytic Design of Linear Feedback Controls, John Wiley & Sons, Inc., New York, 1957.
- J. Gazdag and P. Sguazzero, "Interval Velocity Analysis by Wave Extrapolation," Sixth Year Semi-Annual Progress Review 11, Seismic Acoustics Laboratory, University of Houston, TX, 1983. See also Geophysical Prospecting 32, 454-479 (1984).
- D. Lowe, Ch. 3 in Remote Sensing in Geology, B. S. Siegal and A. R. Gillespie, Eds., John Wiley & Sons, Inc., New York, 1980.
- J. W. Cooley and J. W. Tukey, "An Algorithm for the Machine Calculation of Complex Fourier Series," *Math. Comput.* 19, 297-301 (1965).
- E. O. Brigham, The Fast Fourier Transform, Prentice-Hall Inc., Englewood Cliffs, NJ, 1974.
- J. V. Dave and R. Porinelli, "DIMAPS-II, DIMAPS for IBM 7350," Report No. G320-3432, IBM Scientific Center, Palo Alto, CA. 1982.
- J. Lintz and D. S. Simonett, Eds., Remote Sensing of the Environment, Addison-Wesley Publishing Co., Reading, MA, 1976

Received October 26, 1983; revised February 27, 1984

Jitendra V. Dave IBM Academic Information Systems, 1501 California Avenue, Palo Alto, California 94304. Dr. Dave is at the Palo Alto Scientific Center, on the staff of IBM Fellow H. G. Kolsky. He joined IBM and the Center in 1967 and is currently involved in image processing science and applications. He has worked in atmospheric optics and radiative transfer, remote sensing of atmospheric ozone and aerosols, the effect of particulate contamination on climate, photvoltaic harvesting of solar energy, and large-scale scientific computing through FORTRAN. While on assignment to the Federal Systems Division, Dr. Dave worked on contracts to the NASA Goddard Space Flight Center, Greenbelt, Maryland, for investigations related to the estimation of ozone parameters from the Nimbus-G TOMS measurements. He was also a consultant to the Lawrence Livermore Library, California, for atmospheric radiation transfer problems. Before joining IBM, Dr. Dave was a program scientist at the National Center for Atmospheric Research, Boulder, Colorado, from 1962 to 1967. He was also an Affiliate Associate Professor in the Department of Meteorology at the Florida State University, Tallahassee, from 1966 to 1968. He was principal investigator for the backscatter ultraviolet (BUV) experiment aboard the Nimbus-IV satellite from 1966 to 1967. From 1960 to 1962 he was a research scientist in the Department of Meteorology at Imperial College, London, England. He was a Visiting Assistant Professor and research scientist in the Department of Meteorology at the University of California, Los Angeles, from 1957 to 1960. From 1949 until 1957 he was a research assistant at the Physical Research Laboratory, Ahmedabad, India, Dr. Dave obtained his B.S. in physics and mathematics at Bombay University, India, in 1948, and his M.S. in physics in 1952. He received his Ph.D. in physics from Gujarat University, India, in 1957. Dr. Dave received an IBM Outstanding Contribution Award in 1972 for his work on the influence of atmospheric aerosols on the greenhouse effect. He was elected to the Fellowship of the American Physical Society in 1979.

Jenö Gazdag IBM Academic Information Systems, 1501 California Avenue, Palo Alto, California 94304. Dr. Gazdag received his B.E. from McGill University, Montreal, Canada, in 1959, his M.A.Sc. from the University of Toronto, Canada, in 1961, and his Ph.D. from the University of Illinois, Urbana, in 1966, all in electrical engineering. From 1961 to 1962 he was employed by the National Research Council of Canada in Ottawa. In 1966, he joined IBM's Research Division. He is now manager of engineering and scientific computations at the IBM Scientific Center in Palo Alto. His main research interest is in numerical solution methods for partial differential equations with applications in seismic data processing. Dr. Gazdag is a member of the European Association of Exploration Geophysicists and the Society of Exploration Geophysicists.